Tellus (2000), 52A, 412–421
Printed in UK. All rights reserved

TELLUS
ISSN 0280–6495

Time-space weak-constraint data assimilation for nonlinear models

By FRANCESCO UBOLDI[1]* and MASAFUMI KAMACHI[2], [1]*Magritte s.n.c., corso San Gottardo 41, 20136 Milano MI, Italy;* [2]*Ocean Research Department, Meteorological Research Institute, 1-1 Nagamine, Tsukuba, Ibaraki 305-0052 Japan*

(Manuscript received 21 July 1998; in final form 3 December 1999)

ABSTRACT

A general perturbation–linearization scheme is proposed for the problem of data assimilation with an imperfect and nonlinear model, allowing for the application of the weak constraint representer method. The scheme is shown in discrete formalism for a generic model. An application example is given with computer-generated data in the case of the Burgers equation. Discussion in reference to the assimilation example concerns: the rôle of the model error, seen as a forcing term in the dynamics; the rôle of representers as a posteriori error covariances; a comparison among different choices for a priori dynamic error variance and strong constraint assimilation. Weak and strong constraint methods are also compared in a forecasting experiment.

1. Introduction

Data assimilation methods have recognized and increasing importance in model studies of both the atmosphere and the ocean. These models are characterized by strong nonlinearities, both in the dynamic equations and in the physics parametrization schemes; moreover, nonlinearity may also be involved in the process of estimating, from the model state, the value of an observed variable — the "observation operator". In the following, a general approach to the problem of model nonlinearity is applied to the weak constraint representer method (Bennett, 1992; Bennett et al., 1996, 1997), which includes the strong constraint-4DVAR method (Talagrand and Courtier, 1987) as the particular case in which the model dynamics error is forced to be zero. The approximation proposed in the following is based on the availability of a "good" background trajectory; the solution is then seen as a perturbation of the background trajectory, and the residual from the observations of the background estimate is assumed to be of the same order. In this way the Euler–Lagrange equations, i.e. the components of the penalty function gradient, are linearized around the background trajectory and the representer expansion becomes possible. When restricted to the case of strong constraint assimilation, the present approximation is equivalent to the approximation proposed, as "incremental 4D-VAR" or "4D-PSAS" in Courtier, 1997 (and in Rabier et al. (1998)).

In Section 2, the scheme is shown in a general context with discrete formulation. In Section 3, the scheme is applied to a simple, but strongly nonlinear model: the Burgers equation of a shock wave damped by diffusion, in one space dimension and one velocity variable. An assimilation example is presented there, with data generated from the known analytical solution and pseudo-random errors. In Section 4, strong and weak constraint assimilations are compared in a forecasting experiment with the same model of Section 3.

* Corresponding author.
e-mail: uboldi@magritte.it

2. Representer method for a nonlinear model

At every timestep, $n\,\Delta t$ ($n = 0, \ldots, N$), the model state is a vector, $\boldsymbol{x}_n^{\mathrm{b}}$, of length I. The single timestep model evolution is M:

$$\boldsymbol{x}_n^{\mathrm{b}} = M_{n-1}[\boldsymbol{x}_{n-1}^{\mathrm{b}}]. \tag{2.1}$$

K observations are taken, the kth observation is taken at timestep n_k ($<N$ for simplicity):

$$\boldsymbol{y}^{\mathrm{o}} = [y_1^{\mathrm{o}}, \ldots, y_K^{\mathrm{o}}]^{\mathrm{T}}. \tag{2.2}$$

The observation operator H can be a nonlinear operator. By definition, on the background trajectory:

$$y_k^{\mathrm{b}} \equiv H_k[\boldsymbol{x}_{n_k}^{\mathrm{b}}]. \tag{2.3}$$

The background $\boldsymbol{x}^{\mathrm{b}}$ is an exact model trajectory. A weak type of constraint on the dynamics allows for model error, so the sought solution, $\boldsymbol{x}$ is not an exact model trajectory. A residual, $\boldsymbol{f}$, appears at each timestep as a forcing term in the model equation. Other residuals, $\boldsymbol{i}$ and $\boldsymbol{e}$, are present from the background initial state and from the observations:

$$\boldsymbol{x}_n = M_{n-1}[\boldsymbol{x}_{n-1}] + \boldsymbol{f}_n, \tag{2.4a}$$

$$\boldsymbol{x}_0 = \boldsymbol{x}_0^{\mathrm{b}} + \boldsymbol{i}, \tag{2.4b}$$

$$\boldsymbol{H}_k[\boldsymbol{x}_{n_k}] = y_k^{\mathrm{o}} + e_k. \tag{2.4c}$$

In order to globally minimize all these residuals, the solution is found by minimizing the following penalty function (cost function):

$$\begin{aligned} 2\boldsymbol{J} = &\sum_{n,n'=1}^{N} (\boldsymbol{x}_n - M_{n-1}[\boldsymbol{x}_{n-1}])^{\mathrm{T}} \cdot \boldsymbol{W}_{n,n'}^{\mathrm{d}} \\ &\cdot (\boldsymbol{x}_{n'} - M_{n'-1}[\boldsymbol{x}_{n'-1}]) \\ &+ (\boldsymbol{x}_0 - \boldsymbol{x}_0^{\mathrm{b}})^{\mathrm{T}} \cdot \boldsymbol{B}^{-1} \cdot (\boldsymbol{x}_0 - \boldsymbol{x}_0^{\mathrm{b}}) \\ &+ \sum_{k=1}^{K} (H_k[x_{n_k}] - y_k^{\mathrm{o}})^{\mathrm{T}} \cdot \sigma_0^{-2} \cdot (H_k[\boldsymbol{x}_{n_k}] - y_k^{\mathrm{o}}). \end{aligned} \tag{2.5}$$

It is assumed here, only for simplicity, that observational errors are uncorrelated and have the same variance σ_{o}^2. The $I \times I$ matrix $\boldsymbol{B}$ is the error covariance matrix of the background field at initial time. The $\boldsymbol{W}$'s, $I \times I$ matrices, are defined as "inverse" — as block components of a $(N \cdot I) \times (N \cdot I)$ matrix — of the "dynamics" error covariance matrices:

$$\sum_{n''=1}^{N} \boldsymbol{W}_{n,n''}^{\mathrm{d}} \cdot \boldsymbol{C}_{n'',n'}^{\mathrm{d}} = \boldsymbol{I} \cdot \delta_{n,n'}. \tag{2.6}$$

The adjoint variables are now introduced:

$$\boldsymbol{q}_n \equiv \sum_{n'=1}^{N} \boldsymbol{W}_{n,n'}^{\mathrm{d}} \cdot (\boldsymbol{x}_{n'} - M_{n'-1}[\boldsymbol{x}_{n'-1}]). \tag{2.7}$$

By using the adjoint variables, and setting to zero the first variation of the cost function, the Euler–Lagrange equations (hereafter E–L system), in the variables $\boldsymbol{x}_n$ and $\boldsymbol{q}_n$, are obtained:

$$\begin{cases} \boldsymbol{q}_n = \boldsymbol{M}_n^{\mathrm{T}}(\boldsymbol{x}_n) \cdot \boldsymbol{q}_{n+1} + \sum_{k=1}^{K} \delta_{n,n_k} \cdot \boldsymbol{h}_k(\boldsymbol{x}_{n_k}) \\ \qquad \cdot \sigma_{\mathrm{o}}^{-2} \cdot (y_k^0 - H_k[\boldsymbol{x}_{n_k}]), & (2.8a) \\ \boldsymbol{q}_N = 0; & (2.8b) \end{cases}$$

$$\begin{cases} \boldsymbol{x}_n = M_{n-1}[\boldsymbol{x}_{n-1}] + \sum_{n'=1}^{N} \boldsymbol{C}_{n,n'}^{\mathrm{d}} \cdot \boldsymbol{q}_{n'}, & (2.8c) \\ \boldsymbol{x}_0 = \boldsymbol{x}_0^{\mathrm{b}} + \boldsymbol{B} \cdot \boldsymbol{q}_0, & (2.8d) \end{cases}$$

where $\boldsymbol{M} \equiv M'$ (which is a function of $\boldsymbol{x}$) is the Jacobian matrix of M; its transpose matrix, $\boldsymbol{M}^{\mathrm{T}}$, linearly multiplies the adjoint variable $\boldsymbol{q}$. For each k, the I-vector $\boldsymbol{h}_k$ is the gradient of H_k (or the kth column of $\boldsymbol{H}^{\mathrm{T}}$, transpose Jacobian of H). In the backward evolution equation for $\boldsymbol{q}$, the "adjoint equation" (2.8a), the observations appear in a forcing term. The forward equation for $\boldsymbol{x}$ (2.8c) is the full nonlinear model; here, the model error appears as a forcing term which depends linearly on the adjoint trajectory $\boldsymbol{q}$. This term has been written by inverting (2.7) by means of (2.6). In case the model and the observation operator are linear, the representer method (Bennett 1992) can be applied to decouple and solve the system. Anyhow, this is a nonlinear system both in the forward and in the backward equations. In order to solve the system in an approximate way, the solution and the observed values are written as perturbations of the background trajectory:

$$\boldsymbol{x}_n = \boldsymbol{x}_n^{\mathrm{b}} + \varepsilon \cdot \tilde{\boldsymbol{x}}_n, \tag{2.9a}$$

$$\boldsymbol{q}_n = \varepsilon \cdot \tilde{\boldsymbol{q}}_n, \tag{2.9b}$$

$$y_k^{\mathrm{o}} = H_k[\boldsymbol{x}_{n_k}^{\mathrm{b}}] + \varepsilon \cdot \tilde{\boldsymbol{y}}_k^{\mathrm{o}}. \tag{2.9c}$$

It is assumed here that the background is not far from the sought solution and, by the same order, from the observations. Order zero in ε is the nonlinear model forward evolution, exactly satisfied by the background solution. As a consequence, the adjoint variable is a first order term, so that the error forcing term in the forward equation is zero at zero order. The nonlinear dependence is linearized on the observation operator and on the model 1-step evolution. In the E–L system, zero order terms cancel. After neglecting terms which are second order in ε, the linearized E–L system is obtained in the variables $\tilde{\boldsymbol{x}}$ and $\tilde{\boldsymbol{q}}$:

$$\begin{cases} \tilde{\boldsymbol{q}}_n = \boldsymbol{M}_n^{\mathrm{T}}(\boldsymbol{x}_n^{\mathrm{b}}) \cdot \tilde{\boldsymbol{q}}_{n+1} + \sum_{k=1}^{K} \delta_{n,n_k} \cdot \boldsymbol{h}_k(\boldsymbol{x}_{n_k}^{\mathrm{b}}) \\ \qquad \cdot \sigma_{\mathrm{o}}^{-2} \cdot (\tilde{y}_k^{\mathrm{o}} - \boldsymbol{h}_k(\boldsymbol{x}_{n_k}^{\mathrm{b}})^{\mathrm{T}} \cdot \tilde{\boldsymbol{x}}_{n_k}), & (2.10\mathrm{a}) \\ \tilde{\boldsymbol{q}}_N = 0; & (2.10\mathrm{b}) \end{cases}$$

$$\begin{cases} \tilde{\boldsymbol{x}}_n = \boldsymbol{M}_{n-1}(\boldsymbol{x}_{n-1}^{\mathrm{b}}) \cdot \tilde{\boldsymbol{x}}_{n-1} \\ \qquad + \sum_{n'=1}^{N} \boldsymbol{C}_{n,n'}^{\mathrm{d}} \cdot \tilde{q}_{n'}, & (2.10\mathrm{c}) \\ \tilde{\boldsymbol{x}}_0 = \boldsymbol{B} \cdot \tilde{\boldsymbol{q}}_0. & (2.10\mathrm{d}) \end{cases}$$

The system obtained in this way is linear, since all operators are evaluated on the known background solution. The forward equation is the *forced* tangent linear model, where the forcing term, linear in the adjoint variable, is the first order estimate of the model error. The backward equation is the adjoint, forced by the "observations" term.

The system (2.10) can be decoupled by making use of the representer expansion (Bennett 1992). The method is briefly presented here: a solution is sought in the form:

$$\tilde{\boldsymbol{x}}_n = \sum_{k=1}^{K} \boldsymbol{r}_n^k \cdot \beta_k, \tag{2.11a}$$

$$\tilde{\boldsymbol{q}}_n = \sum_{k=1}^{K} \boldsymbol{a}_n^k \cdot \beta_k. \tag{2.11b}$$

The I-vectors $\boldsymbol{r}^k$ are the representers and the I-vectors $\boldsymbol{a}^k$ are the adjoint representers. The β_k coefficients are chosen so that $\boldsymbol{r}^k$ and $\boldsymbol{a}^k$ are solutions of the system:

$$\begin{cases} \boldsymbol{a}_n^k = \boldsymbol{M}_n^{\mathrm{T}}(\boldsymbol{x}_n^b) \cdot \boldsymbol{a}_{n+1}^k + \delta_{n,n_k} \cdot \boldsymbol{h}_k(\boldsymbol{x}_{n_k}^{\mathrm{b}}), & (2.12\mathrm{a}) \\ \boldsymbol{a}_N^k = 0; & (2.12\mathrm{b}) \end{cases}$$

$$\begin{cases} \boldsymbol{r}_n^k = \boldsymbol{M}_{n-1}(\boldsymbol{x}_{n-1}^{\mathrm{b}}) \cdot \boldsymbol{r}_{n-1}^k + \sum_{n'=1}^{N} \boldsymbol{C}_{n,n'}^{\mathrm{d}} \cdot \boldsymbol{a}_{n'}^k, & (2.12\mathrm{c}) \\ \boldsymbol{r}_0^k = \boldsymbol{B} \cdot \boldsymbol{a}_0^k, & (2.12\mathrm{d}) \end{cases}$$

which can be solved for each k by integrating backward first, then forward.

In order to write the system (2.12), the β_k coefficients have to be chosen so that:

$$\boldsymbol{b} = \varepsilon^{-1} \cdot (\boldsymbol{R} + \boldsymbol{S})^{-1} \cdot (\boldsymbol{y}^{\mathrm{o}} - \boldsymbol{y}^{\mathrm{b}}). \tag{2.13}$$

With the following definitions:

$\boldsymbol{b}^{\mathrm{T}} = [\beta_1, \ldots, \beta_K]^{\mathrm{T}}$ K-vector (2.14a)

$\boldsymbol{G}_n = [\boldsymbol{r}_n^1, \ldots, \boldsymbol{r}_n^K]$ $(I \times K)$-matrix (2.14b)

$\boldsymbol{A}_n = [\boldsymbol{a}_n^1, \ldots, \boldsymbol{a}_n^K]$ $(I \times K)$-matrix (2.14c)

$\boldsymbol{R} = \sigma_0^2 \cdot \boldsymbol{I}$ $(K \times K)$-matrix (2.14d)

$[\boldsymbol{S}]_{k,m} = (\boldsymbol{h}_k(\boldsymbol{x}_{n_k}^{\mathrm{b}}))^{\mathrm{T}} \cdot \boldsymbol{r}_{n_k}^{\mathrm{m}}$ k, m component of a $(K \times K)$-matrix. (2.14e)

By substituting back in the (2.11), the solution can be explicitly written:

$$\boldsymbol{x}_n = \boldsymbol{x}_n^{\mathrm{b}} + \boldsymbol{G}_n \cdot (\boldsymbol{R} + \boldsymbol{S})^{-1} \cdot (\boldsymbol{y}^{\mathrm{o}} - \boldsymbol{y}^{\mathrm{b}}). \tag{2.15}$$

This is the expression of an "optimal interpolation" analysis (Daley, 1991; Lorenc, 1986) in space and time (4*D*-OI), where the K representers $\boldsymbol{r}^k$, taken together, form the analysis–observation background field error covariance matrix $\boldsymbol{G}_n$; $\boldsymbol{R}$ is the observation error covariance matrix, and $\boldsymbol{S}$, the $K \times K$ matrix built by applying the linearized observation operator to the representers, is the "observation estimate from background field" error covariance matrix. Thus, the solution of the linearized E–L system can be seen as a 4*D*-OI analysis, where the tangent linear model and its adjoint are used to compute the a posteriori covariance matrices, $\boldsymbol{G}_n$ and $\boldsymbol{S}$, starting from the a priori covariances $\boldsymbol{B}$ and $\boldsymbol{C}^{\mathrm{d}}$. The single kth representer, which is a function of space and time (i.e., an $(I \cdot N)$ vector), can be seen as the a posteriori, "OI" covariance function for the kth observation. The properties of this covariance are discussed, with reference to an application example, in Section 3.

The following procedure (Egbert and Bennett, 1994) is presented here for a complete description of the method used in the present work. In order to find the "weak constraint" solution (2.15), the K-order linear equation:

$$(\boldsymbol{R} + \boldsymbol{S}) \cdot \boldsymbol{z} = (\boldsymbol{y}^{\mathrm{o}} - \boldsymbol{y}^{\mathrm{b}}) \tag{2.16}$$

has to be solved with respect to z. Its solution is a zero of the gradient of the function:

$$F(z) = \tfrac{1}{2} z^{\mathrm{T}} \cdot (\boldsymbol{R} + \boldsymbol{S}) \cdot z - z^{\mathrm{T}} \cdot (y^{\mathrm{o}} - y^{\mathrm{b}}), \tag{2.17}$$

which can be minimized by using the conjugate gradient iteration (Press et al., 1992). In order to do so, since the observation covariance $\boldsymbol{R}$ is known, it is necessary to evaluate $\boldsymbol{S} \cdot \boldsymbol{w}$ on an arbitrary K-vector $\boldsymbol{w}$. This is obtained by multiplying $\boldsymbol{h}_k^{\mathrm{T}}$, as done in (2.14e), to the forward solution $\boldsymbol{s}$ of the linear system (compare with (2.10)):

$$\begin{cases} \boldsymbol{p}_n = \boldsymbol{M}_n^{\mathrm{T}}(\boldsymbol{x}_n^{\mathrm{b}}) \cdot \boldsymbol{p}_{n+1} \\ \qquad + \sum\limits_{k=1}^{K} \delta_{n,n_k} \cdot \boldsymbol{h}_k(\boldsymbol{x}_{n_k}^{\mathrm{b}}) \cdot w_k, & (2.18\mathrm{a}) \\ \boldsymbol{p}_N = 0; & (2.18\mathrm{b}) \end{cases}$$

$$\begin{cases} \boldsymbol{s}_n = \boldsymbol{M}_{n-1}(\boldsymbol{x}_{n-1}^{\mathrm{b}}) \cdot \boldsymbol{s}_{n-1} \\ \qquad + \sum\limits_{n'=1}^{N} \boldsymbol{C}_{n,n'}^{\mathrm{d}} \cdot \boldsymbol{p}_{n'}, & (2.18\mathrm{c}) \\ \boldsymbol{s}_0 = \boldsymbol{B} \cdot \boldsymbol{a}_0, & (2.18\mathrm{d}) \end{cases}$$

where $\boldsymbol{p}_n$ and $\boldsymbol{s}_n$ are auxiliary I-vectors.

The backward and forward integrations in (2.18) are performed at every step of the conjugate gradient iteration. The iteration is carried on until the relative error in the K-order linear equation is less than a threshold, set in the application to 10^{-6}, corresponding to the linearized gradient "zero" value reported in Section 3.

3. Application of the assimilation scheme to the Burgers equation

The Burgers equation describes a shock wave damped by diffusion; it was already chosen to test a different data assimilation method (Menard, 1994):

$$\begin{cases} \dfrac{\partial u}{\partial t} + u \dfrac{\partial u}{\partial x} = \kappa \dfrac{\partial^2 u}{\partial x^2}, & (3.1\mathrm{a}) \\ u(x, 0) = U(x). & (3.1\mathrm{b}) \end{cases}$$

The analytical solution of the Burgers equation is known (e.g., Whitham, 1974; see also here, Section 6). The numerical model is defined as a finite-difference leapfrog scheme, with a forward step every 15 timesteps. If an initial condition is chosen to be zero outside an interval $[-L, L]$, the numerical solution remains zero during the time interval $[0, T]$ outside a (wider) interval $[-X, X]$ which can be chosen as integration domain with constant and equal to zero boundary conditions.

Model parameters are: $\Delta t = 60$ s; $\Delta x = 5$ km; $\mathrm{IM} = 200$, $X = \mathrm{IM} \cdot \Delta x = 1000$ km, grid points are defined for $i = -\mathrm{IM}, \ldots, \mathrm{IM}$; $N = 960$, $T = N \cdot \Delta t = 16$ h, timesteps are defined for $n = 0, \ldots, N$; $\kappa = 1.4 \cdot 10^4\ \mathrm{m^2\,s^{-1}}$ in the numerical model; $\kappa = 1{\cdot}0 \cdot 10^4\ \mathrm{m^2\,s^{-1}}$ in the analytical solution.

The observation operator is a linear interpolation between the nearest neighbours gridpoints, so it is a linear operator, and it is particularly simple.

The initial condition is shown in Fig. 1 together with other states of the analytical solution. With $U_0 = 5\ \mathrm{m\,s^{-1}}$ and $L = 50$ km, it is defined by:

$$\begin{cases} U(x) = 0 & |x| \geqslant L \\ U(x) = U_0 \left(1 + 2\dfrac{|x|}{L}\right)\left(1 - \dfrac{|x|}{L}\right)^2 & |x| < L. \end{cases} \tag{3.6}$$

The analytical solution is considered here the "true" solution; it is shown in Fig. 1 (velocity profiles at various times) and Fig. 2 (contour lines in the x–t plane).

The aim of the experiment is to study the correcting effect of the assimilation on the model error in the case of a simple, nonlinear, imperfect model.

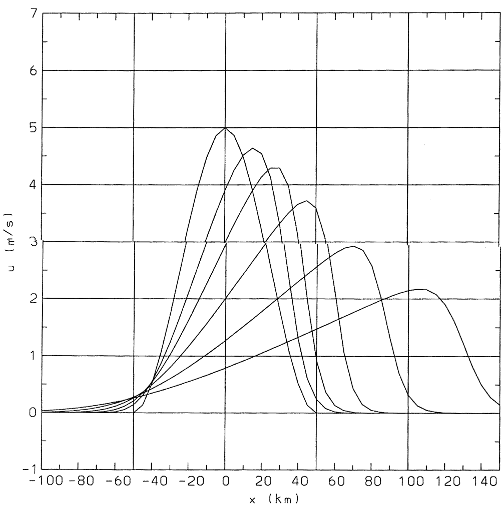

Fig. 1. Analytical solution at times 0 h (initial condition), 1 h, 2 h, 4 h, 8 h, 16 h.

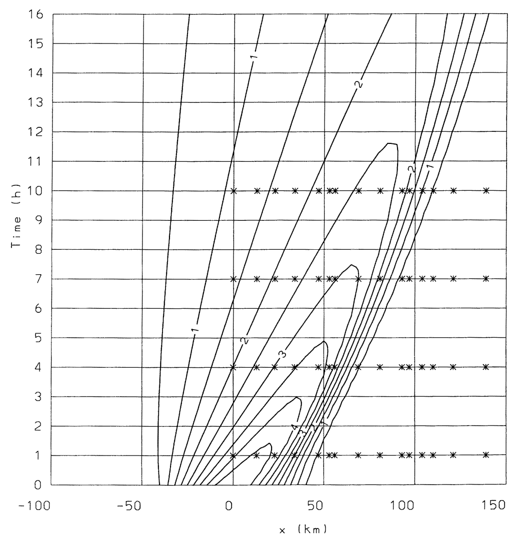

Fig. 2. Analytical solution in the x–t plane. Asterisks mark observation locations.

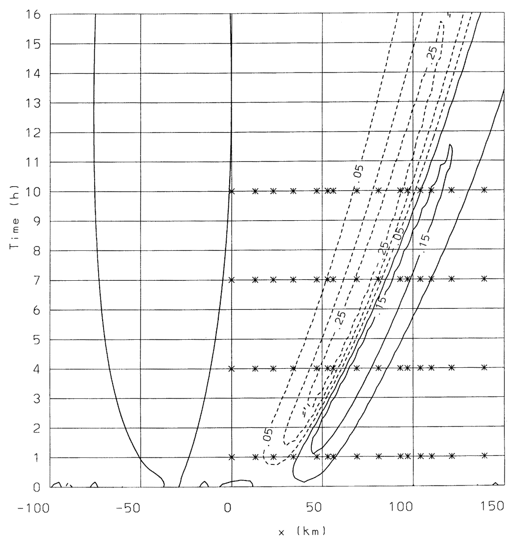

Fig. 3. Difference between background trajectory and analytical solution.

The choice made for the model error is to use a "wrong" value for the diffusivity coefficient, i.e., different from the one used in the analytical solution. The idea is that most of the errors usually present in the models are systematic, but unknown. The value of the diffusivity coefficient has been chosen to be $\kappa = 1.4 \cdot 10^4\ \mathrm{m^2\ s^{-1}}$ in order to provide a small difference with the "true" value, $\kappa = 1.0 \cdot 10^4\ \mathrm{m^2\ s^{-1}}$. This error is comparable with, or even smaller than errors believed to be present in the models of the atmosphere and the ocean.

The initial condition for the numerical integration is obtained by adding a normally distributed error to the initial condition of the analytical solution. The variance of this synthetic error is $\sigma_i^2 = (10^{-2} U_0)^2 = 2.5 \cdot 10^{-3}\ \mathrm{m^2\ s^{-2}}$.

The integration of the non-linear numerical model gives the background solution: its difference from the analytical solution is shown, through contour lines in the x–t plane, in Fig. 3. The different value of the diffusivity coefficient determines a difference in the intensity of the shock front.

60 observations are estimated by applying the observation operator to the analytical solution and adding a normally distributed error with variance $\sigma_o^2 = (10^{-2} U_0)^2 = \sigma_i^2$. The observations are referred to 4 different times: $+1$ h, $+4$ h, $+7$ h, $+10$ h. The locations of the observations are irregularly distributed in the positive-x region, where the shock front moves during the assimilation period. The irregularity of their distribution is such that the sharp front only occasionally is accurately resolved. Observation locations are marked with asterisks in Figs. 2, 3, 5, 6, 7.

The assimilation method described in Section 2 is applied. The model equations are linearized around the background solution, and the resulting linear system is solved by applying the representer method and the Egbert–Bennett iterative conjugate gradient scheme.

The a priori choice for observation errors, as in Section 2, is that they are uncorrelated, and characterized by the same known variance, σ_o^2.

The components of the initial error covariance matrix $\boldsymbol{B}$ are estimated by a Gaussian exponential of the distance between gridpoints, with decorrelation scale 12 km; the known variance is σ_i^2.

The space–time dynamics errors covariance matrix's elements are factorized in space and time parts, each being a Gaussian exponential with scales 12 km and 1.5 h respectively; the variance is σ_d^2.

The choice of the space and time scale parameters is aimed at (approximately) resolving the smallest scales compatible with the distribution of observation locations and times.

The choice of dynamic error variance σ_d^2 is

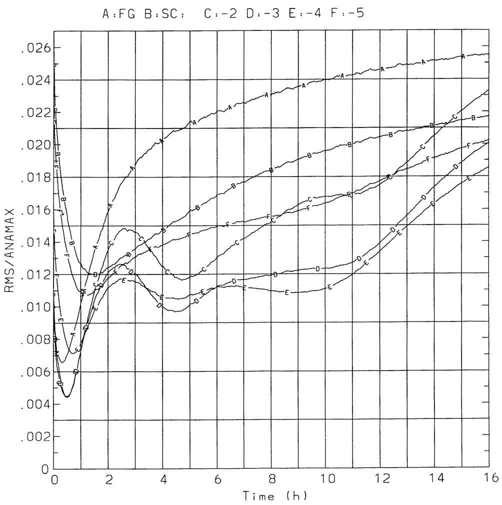

Fig. 4. Relative root-mean-square residual from analytical solution versus integration time. Curve A: background trajectory; curve B: strong constraint assimilation; curves C to F: weak constraint assimilation with different values of a priori dynamic error variance, with ratio σ_d^2/σ_i^2 as follows: C: 10^{-2}; D: 10^{-3}; E: 10^{-4}; F: 10^{-5}.

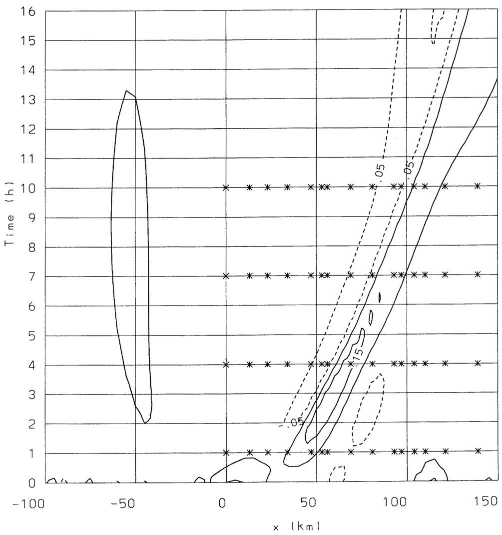

Fig. 5. Difference between solution after assimilation and analytical solution.

briefly discussed here. By keeping constant the (supposed known) "observations" and "initial condition" variances $\sigma_o^2 = \sigma_i^2 = (10^{-2} U_0)^2$, the weak constraint assimilation has been computed for

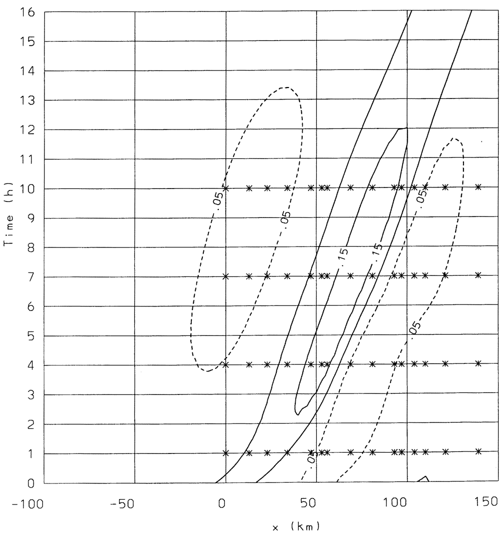

Fig. 6. Difference between solution and background trajectory.

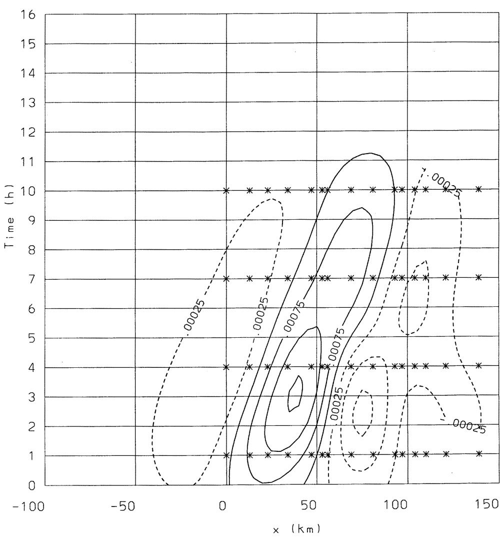

Fig. 7. Error forcing for the solution.

different orders of magnitude of σ_d^2, ranging from $\sigma_d^2 = 10^{-2}\sigma_i^2$ to $\sigma_d^2 = 10^{-5}\sigma_i^2$. The strong constraint assimilation, $\sigma_d^2 = 0$, has also been computed.

The root-mean-square residual (RMS) from the analytical solution has been calculated at each timestep. By effect of the linear diffusion term the values of the solutions decrease in time everywhere; as a consequence, all the RMS also decrease in time. For this reason the ratio between the RMS and the instantaneous maximum of the analytical solution has been calculated at each timestep. Fig. 4 shows the values of this relative RMS for the background trajectory, for the strong constraint assimilation, and for different choices of a priori dynamic error variance in weak constraint assimilation.

Bigger values of σ_d^2 (curves C and D) show wider oscillations corresponding to observation times. Smaller values of σ_d^2 (F) approach the strong constraint curve (B). The best among the plotted curves (E) is obtained when $\sigma_d^2 = 10^{-4}\sigma_i^2 = 10^{-4}\sigma_o^2$. All assimilations have errors smaller than the background trajectory in the whole assimilation interval. Weak constraint assimilation provide better results than strong constraint during the assimilation interval for a very wide range of values (orders of magnitude) of the "dynamics" variance. The "E" variance, $\sigma_d^2 = 10^{-4}\sigma_i^2$, is chosen for the following discussion and for a forecasting experiment (Section 4).

The solution obtained after assimilating the observations is shown in Fig. 5, difference from the analytical solution, and in Fig. 6, difference from the background trajectory. Comparison between Fig. 5 and Fig. 3 shows the reduction of the error after the assimilation, and Fig. 6 shows that the correction to the background trajectory is correctly distributed in the frontal (space-time) region where the background error is located.

Table 1 shows the value of the cost function and the modulus of its gradient as evaluated on the background trajectory and after assimilation. J_d, J_i and J_o are the "dynamic", "initial condition" and "observation" terms in the cost function, i.e., the 1st, 2nd and 3rd terms in (2.5). As a comparison for the gradient norm values, the norm of the linearized gradient (considered zero) is $2.761 \cdot 10^{-4}\,\mathrm{s\,m^{-1}}$ after the conjugate gradient iteration (Section 2).

The error forcing term for the solution is shown in Fig. 7. This is the model error estimate, obtained by convolution between dynamics covariance and adjoint variable. Out of time–space areas characterized by nonzero value of the adjoint variables, the error forcing term approaches zero with the time and space scales set in the a priori covariance functions. In particular, it is still significantly nonzero after the last observation time.

The representers, i.e., the a posteriori covariance functions for single observations, have been separately calculated by integrating first the backward eq. (2.12a), then the forward eq. (2.12c), forced by the time-space convolution of the adjoint representer with the a priori covariance. Fig. 8 shows this error forcing field for the representer $m = 57$. Since when the forcing has gradually vanished after the observation time, the representer evolves as a free solution of the linearized forward equation. The trajectory of the representer $m = 57$ is shown in Fig. 9 until $+60$ h, i.e., much later than the time, $+10$ h, of the 57th observation, marked by the black dot in the figure.

The weak constraint solution can be seen as a particular "4D optimal interpolation". So, from

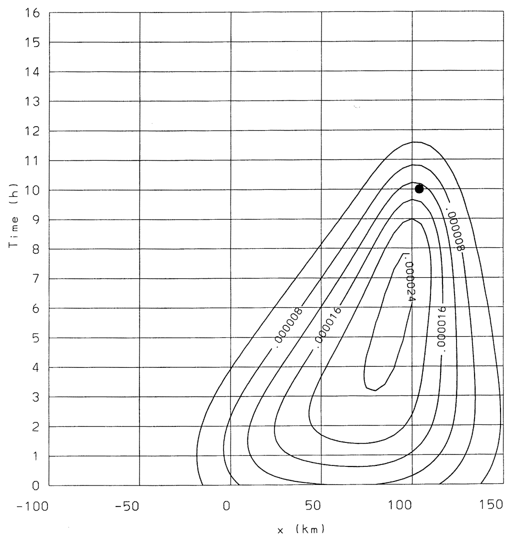

Fig. 8. Error forcing for representer $m = 57$. Black dot marks location of observation $m = 57$.

Table 1.

J	J_d	J_i	J_o	$\lvert\nabla J\rvert$ ($\mathrm{s\,m^{-1}}$)	... evaluated on:
178.5	0.0	0.0	178.5	336.1	background trajectory
78.54	22.04	2.903	53.59	1.132	solution after assimilation

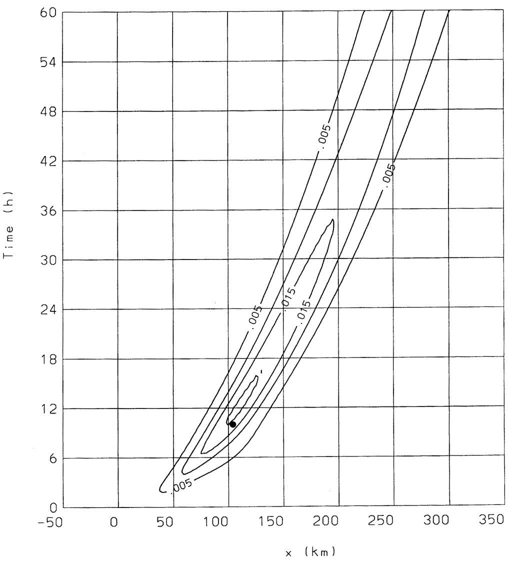

Fig. 9. Representer $m = 57$ until $+60$ h. Black dot marks location of observation $m = 57$.

an "optimal interpolation" point of view, one might expect that the solution approaches the background field in areas which are far, in space or in time, from the observations. Nevertheless, as integration time proceeds, the a posteriori covariance — the representer — does not go to zero as a Gaussian covariance would do. As a consequence, the solution does not necessarily approach the background trajectory after the assimilation interval. The two trajectories are separated, once and for all, by the error forcing, which is active in the assimilation period. When the forcing term vanishes, the solution is free to evolve, in particular it evolves separately from the background trajectory.

4. Comparison between weak and strong constraint in a forecast experiment

Eknes and Evensen (1995) performed a weak constraint assimilation experiment, in the linear case, by using a model which was previously used for a strong constraint assimilation experiment. A comparison between weak and strong constraint assimilation is done here with the purpose of enhancing how the difference in the two approaches affects the forecast results in a case where a model error is explicitly introduced, as explained in Section 3, in the dynamics of a simple but nonlinear model.

Result of a strong constraint assimilation is a correction of the initial condition. Result of a weak constraint assimilation is an estimate of the model error in the assimilation interval, i.e., a correction of the model trajectory — the "error forcing term". A forecasting simulation is realized, in the strong constraint case, by running the full nonlinear model from the new initial condition. In the weak constraint case, a forecasting simulation is realized by adding the estimate of the model error to the full nonlinear model evolution at each timestep during the assimilation interval. By using the fields computed as explained in Section 3 ("E" variance), a forecasting simulation was realized in both cases, "strong" and "weak" constraint. The initial condition computed after strong constraint assimilation is shown in Fig. 10, with the "true" initial condition, used for the analytical solution. The error forcing computed after weak constraint assimilation is shown in Fig. 7. This field starts to gradually vanish when observations are not available anymore, after the last one at $+10$ h. Since the error is estimated as a convolution between a priori covariances and adjoint variables (which are zero after the last

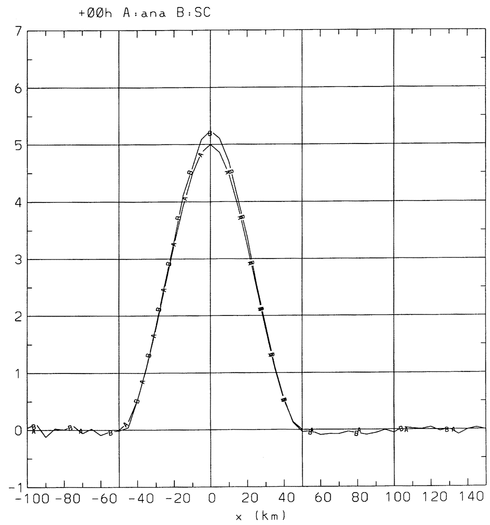

Fig. 10. Initial condition for analytical solution (curve A, same as in Fig. 1) and for solution after strong constraint assimilation (curve B).

observation), the error forcing vanishes after the last observation time with the time scale set in the a priori time covariance function (1.5 h). The error forcing term is considered reasonably close to zero at the end of the assimilation interval, +16 h. Since then, the model is free to evolve. The simulation is extended in time until +60 h.

A relative RMS (computed as explained for Fig. 4) is plotted in Fig. 11 for the three solutions: background, strong constraint and weak constraint. Both "strong" and "weak" solutions have a smaller error than the background trajectory until the end of the simulation. The strong constraint solution has a larger error at time zero. This can be understood because the residuals between background estimates and observations are not only due to errors in the initial condition, but to the error present in the model dynamics, too. The weak constraint solution has a very small error during the whole assimilation period; it is still significantly smaller than the strong constraint solution error for an interval, after the last observation time, of about 10–15 h, which is much longer than the time scale (1.5 h) used in the Gaussian a priori covariance: this improvement is due to the action of the error forcing term, active only during the assimilation period, on the model evolution. Later, say after +25h, the error curves approach each other until the end of the simulation because of the damping effects of linear diffusion.

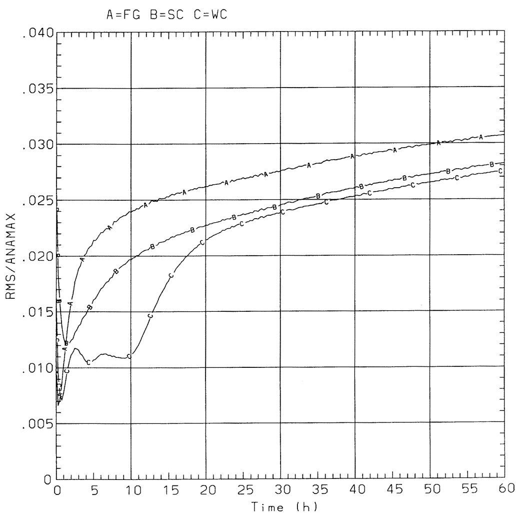

Fig. 11. Relative root-mean-square residual from analytical solution versus integration time. Curve A: background trajectory; curve B: strong constraint; curve C: weak constraint assimilation.

5. Acknowledgements.

One of us (F. Uboldi) attended the 1997 Summer School on "Inverse Methods and Data Assimilation", held at Oregon State University — College of Oceanic and Atmospheric Sciences, by Andrew F. Bennett, whom we thank for the extreme clarity in presenting the linear representer method, for the useful comments about data assimilation methods, and for the very efficient-but-kind organization. We also thank Anna Trevisan of CNR-ISAO, Bologna (Italy) for useful discussion of the revised version of the paper. A part of this work is supported by CREST (Core Research for Evolutional Science and Technology) of Japan Science and Technology Corporation (JST).

6. Appendix

Evaluation of the analytical solution of the Burgers equation

By assuming that the solution and its space derivatives go to zero quickly enough when x goes to infinite, the Burgers equation has the following solution (Whitham, 1974):

$$u(x,t) = \frac{\displaystyle\int_{-\infty}^{+\infty} \frac{x-\xi}{t}\, e^{-(1/2\kappa)[P(\xi)+(x-\xi)^2/2t]}\, d\xi}{\displaystyle\int_{-\infty}^{+\infty} e^{-(1/2\kappa)[P(\xi)+(x-\xi)^2/2t]}\, d\xi}, \tag{6.1}$$

where the primitive function of the initial condition appears:

$$P(x) = \int_0^x U(\eta)\, d\eta, \tag{6.2}$$

which, for the initial condition chosen in Section 3, can be calculated analytically. The solution can be transformed to:

$$u(x,t) = \frac{\displaystyle\int_{-\infty}^{+\infty} \frac{\xi}{t} \left(e^{-(1/2\kappa)[P(x-\xi)+\xi^2/2t]} - e^{-(1/2\kappa)[P(x+\xi)+\xi^2/2t]}\right) d\xi}{\displaystyle\int_{0}^{+\infty} \left(e^{-(1/2\kappa)[P(x-\xi)+\xi^2/2t]} + e^{-(1/2\kappa)[P(x+\xi)+\xi^2/2t]}\right) d\xi} \tag{6.3}$$

This expression can be discretized as:

$$u(x,t) \cong \frac{\Delta\xi}{t} \frac{\displaystyle\sum_{j=1}^{+\infty} j\, e^{-(1/2\kappa)[P(x-j\Delta\xi)+j^2\Delta\xi^2/2t]} - \sum_{j=1}^{+\infty} j\, e^{-(1/2\kappa)[P(x+j\Delta\xi)+j^2\Delta\xi^2/2t]}}{\displaystyle e^{-(1/2\kappa)P(x)} + \sum_{j=1}^{+\infty} e^{-(1/2\kappa)[P(x-j\Delta\xi)+j^2\Delta\xi^2/2t]} + \sum_{j=1}^{+\infty} e^{-(1/2\kappa)[P(x+j\Delta\xi)+j^2\Delta\xi^2/2t]}}, \tag{6.4}$$

where $\xi = j\Delta\xi$. Each series has to be numerically evaluated by computing a finite number of terms. Thus, two different approximations are used: the first is given by the size of $\Delta\xi$; the second by the number of terms which are actually computed to evaluate the series. In order to estimate the number of terms required in the evaluation, one notes that each term is dominated by the product of two exponentials: one is a Gaussian of the index j; the maximum value of the other one, if the initial condition of Section 3 is chosen, is $\exp(U_0 L/4\kappa)$, which is dominated by the Gaussian (i.e. the product can be considered to be zero) when $j > \sqrt{(U_0 L + 4\alpha\kappa)t}/\Delta\xi$, where α is chosen so that $e^{-\alpha}$ is reasonably close to zero.

The values chosen for the parameters are: $U_0 = 5\ \mathrm{m\,s^{-1}}$; $L = 50$ km; $\Delta x = 5$ km; $\Delta t = 60$ s; $\kappa = 1.0 \cdot 10^4\ \mathrm{m^2\,s^{-1}}$; $\Delta\xi = 0.5\ \mathrm{km} = 0.1\Delta x$; $\alpha = 36$.

REFERENCES

Bennett, A. F. 1992. *Inverse methods in physical oceanography.* Cambridge University Press, 346 pp.

Bennett, A. F., Chua, B. and Leslie, L. 1996. Generalized inversion of a global numerical weather prediction model. *Meteorol. Atmos. Phys.* **60**, 165–178.

Bennett, A. F., Chua, B. and Leslie, L. 1997. Generalized inversion of a global numerical weather prediction model (II). Analysis and implementation. *Meteorol. Atmos. Phys.* **62**, 129–140.

Courtier, P. 1997. Dual formulation of four-dimensional variational assimilation. *Quart. J. Roy. Meteor. Soc.* **123**, 2449–2461.

Courtier, P. and Talagrand, O. 1987. Variational assimilation of meteorological observations with the adjoint vorticity equation (I). Theory. *Quart. J. Roy. Meteor. Soc.* **113**, 1311–1328.

Daley, R. A. 1991. *Atmospheric data analysis.* Cambridge University Press, 457 pp.

Egbert, G. and Bennett, A. F. 1994. Topex/Poseidon tides estimated using a global inverse model. *J. Geophys. Res.* **99**, 24821–24852.

Eknes, M. and Evensen, G. 1995. Parameter estimation solving a weak constraint variational problem. *Proceedings of WMO's 2nd International Symposium on Assimilation of observations in meteorology and oceanography*, March 1995. Tokyo, Japan; PWPR report series no. 5; WMO/TD- no. 651; Vol. I, pp. 95–97.

Ide, K., Courtier, P., Ghil, M. and Lorenc, A. 1997. Unified notation for data assimilation: operational, sequential and variational. *J. Meteorol. Soc. Japan* **75**, 181–189.

Lorenc, A. C. 1986. Analysis methods for numerical weather prediction. *Quart. J. Roy. Meteor. Soc.* **112**, 1177–1194.

Menard, R. 1994. *Kalman filtering of Burgers' equation and its application to atmospheric data assimilation.* PhD Thesis at McGill University. Stormy Weather Group, Scientific Report MW-100, Montreal, Canada, 210 pp.

Press, W. H., Flannery, B. P., Teukolsky, S. A. and Vetterling, W. T. 1992. *Numerical recipes, the art of scientific computing.* Cambridge University Press, 702 pp.

Rabier, F., Thépaut, J-N. and Courtier, P. 1998. Extended assimilation and forecast experiments with a four-dimensional variational assimilation system. *Quart. J. Roy. Meteor. Soc.* **124**, 1861–1887.

Whitham, G. B. 1974. *Linear and nonlinear waves.* John Wiley and Sons, 636 pp.